NANO LETTERS

2008
Vol. 8, No. 8
2423-2431

Photonic-Plasmonic Scattering Resonances in Deterministic Aperiodic Structures

Ashwin Gopinath,[†] Svetlana V. Boriskina,[†] Ning-Ning Feng,[†] Björn M. Reinhard,[‡] and Luca Dal Negro*[,†]

Department of Electrical and Computer Engineering, Boston University, 8 Saint Mary's Street, Boston, Massachusetts 02215-2421, and Department of Chemistry, Boston University, 590 Commonwealth Avenue, Boston, Massachusetts 02215

Received May 13, 2008; Revised Manuscript Received June 21, 2008

ABSTRACT

In this paper, we combine experimental dark-field scattering spectroscopy and accurate electrodynamics calculations to investigate the scattering properties of two-dimensional plasmonic lattices based on the concept of aperiodic order. In particular, by discussing visible light scattering from periodic, Fibonacci, Thue−Morse and Rudin−Shapiro lattices fabricated by electron-beam lithography on transparent quartz substrates, we demonstrate that deterministic aperiodic Au nanoparticle arrays give rise to broad plasmonic resonances spanning the entire visible spectrum. In addition, we show that far-field diffractive coupling is responsible for the formation of characteristic photonic-plasmonic scattering modes in aperiodic arrays of metal nanoparticles. Accurate scattering simulations based on the generalized Mie theory approach support our experimental results. The possibility of engineering complex metal nanoparticle arrays with distinctive plasmonic resonances extending across the entire visible spectrum can have a significant impact on the design and fabrication of novel nanodevices based on broadband plasmonic enhancement.

The control of light−matter interaction in deterministic media without translational invariance offers an almost unexplored potential for the creation and manipulation of highly confined optical fields. Unlike periodic photonic structures, deterministic aperiodic structures (DAS) possess unique light localization and anomalous transport properties related to far richer spectral features described by multifractal energy spectra.[1–5] However, unlike random media, DAS are defined by the iteration of simple mathematical rules, rooted in symbolic dynamics,[6] prime number theory[7] and L-system inflations,[8] which can encode a fascinating complexity. In particular, DAS share distinctive physical properties with both periodic media, i.e., the formation of well-defined energy gaps, and disordered random media, i.e., the presence of localized eigenstates with high field enhancement. Until now, the study of optical DAS has been mainly limited to one-dimensional (1D) systems with quasi-periodic modulation of their optical constants, such as Fibonacci[9–11] and Cantor-set multilayer structures.[12] However, electromagnetic scattering, plasmon localization and band gap formation in one and two-dimensional arrays of metal nanoparticles with deterministic aperiodic geometries have been recently discussed, and broad plasmon scattering spectra have been predicted on the basis of coupled-dipole calculations.[13–15] In this paper, we combine dark-field scattering spectroscopy and accurate Mie-theory calculations to study the far-field scattering characteristics of two-dimensional Au nanoparticle arrays based on Fibonacci, Thue−Morse and Rudin−Shapiro aperiodic sequences. These structures are the most thoroughly investigated examples of deterministic nonperiodic systems and are characterized by quasi-periodic, singular-continuous and absolutely continuous Fourier spectra, respectively.

Fibonacci quasi-crystals are the well-known paradigms of quasi-periodic order and in one spatial dimension can be obtained by combining two different optical materials A and B according to the inflation rule: A → AB, B → A.[16] Since the first experimental realization of a dielectric Fibonacci quasi-crystal by Gellermann et al.,[17] Fibonacci systems have been intensively investigated, leading to the experimental demonstration of transmission scaling,[18] symmetry induced resonances,[19] nonlinear coupling enhancement[20] and strong group velocity suppression at the fractal band-edge modes.[21,22] Recently, highly localized plasmon modes (hot-spots) with strong field enhancement have been demonstrated in two-dimensional (2D) Fibonacci arrays of metal nanoparticles, and the formation of plasmonic pseudogaps has been shown in Fibonacci-modulated nanoparticle chains.[13,14]

More complex aperiodic structures are characterized by singular-continuous and absolutely continuous Fourier spectra.

* Corresponding author. E-mail: dalnegro@bu.edu.
† Department of Electrical and Computer Engineering.
‡ Department of Chemistry.

10.1021/nl8013692 CCC: $40.75
Published on Web 07/23/2008

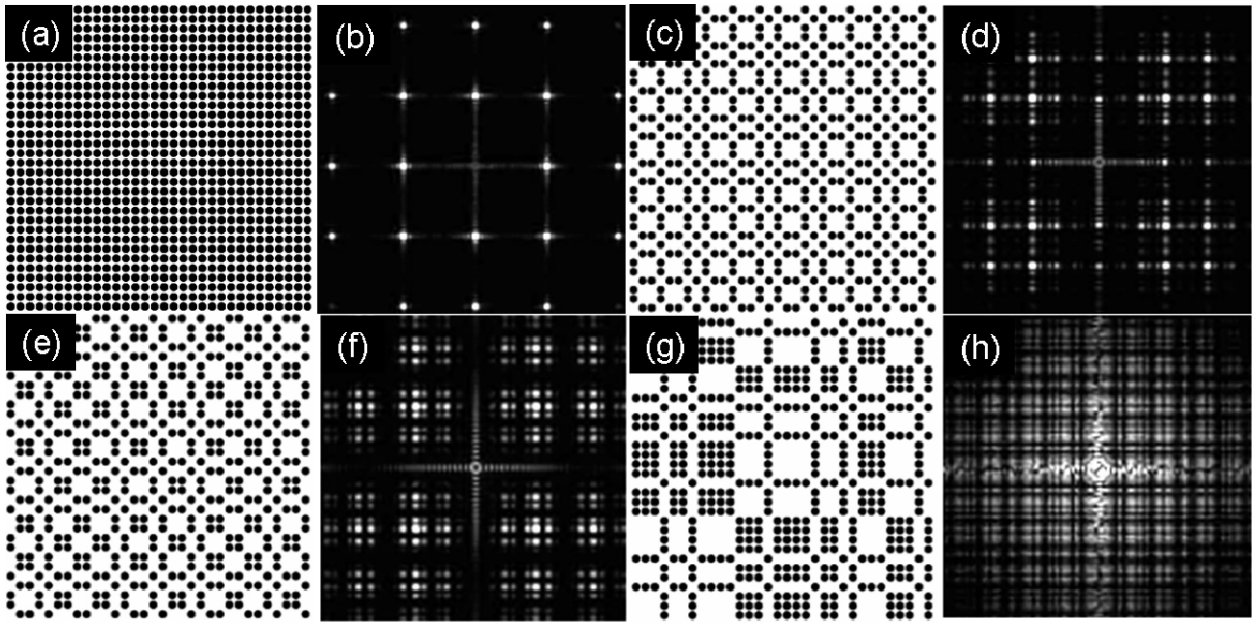

Figure 1. Two-dimenional (2D) lattices calculated after seven iterations of the algorithm in ref 15: (a) periodic 2D sequence (square array), (c) Fibonacci 2D sequence, (e) Thue−Morse 2D sequence, (g) Rudin−shapiro 2D sequence. The black circles represent arbitrary metal nanoparticles arranged in the direct (real) space. Calculated 2D diffraction patterns (reciprocal space representations) of the (b) periodic, (d) Fibonacci, (f) Thue−Morse, and (h) and Rudin−Shapiro lattices.

The principal example of singular-continuous deterministic systems is given by the Thue−Morse sequence, which in one spatial dimension can be generated by the simple inflation rule: A → AB, B → BA.[23] The Thue−Morse sequence has been extensively investigated in the mathematical literature as the prototype of substitutional aperiodic symbolic maps which give rise to multifractal Fourier spectra and aperiodic attractors.[24–26] So far only one-dimensional optical structures based on the Thue−Morse sequence have been experimentally investigated. These studies revealed that multiple wave scattering in Thue−Morse structures gives rise to a self-similar hierarchy of pseudoband-gap regions, which support resonant states with large field enhancement.[27,28] Omnidirectional reflectivity and light emission enhancement in Thue−Morse structures have also been recently demonstrated.[28,29]

The more general category of deterministic aperiodic systems includes sequences whose Fourier spectra have an absolutely continuous character, akin to purely random structures with white spectra. These structures share most of their physical properties with random media, such as the presence of exponentially localized light states, and subdiffusive light transport.[30,31] The primary example of this fascinating category of aperiodic structures is the Rudin−Shapiro sequence. In a two-letter alphabet, the RS sequence can simply be obtained by the iteration of the two-letter inflation: AA → AAAB, AB → AABA, BA → BBAB, BB → BBBA.[3,32] It is interesting to mention that even for one spatial dimension, there is presently no complete agreement on the localization character of the Rudin−Shapiro eigenmodes, and it has been recently pointed out that extended states coexist with exponentially localized ones.[32,33]

With the goal of investigating light scattering from aperiodic arrays, we have recently shown that simple inflation methods exist to generalize well-known 1D aperiodic sequences into higher spatial dimensions.[15] Following this approach, 2D aperiodic arrays of metal nanoparticles with different spectral properties can be fabricated using well-established top-down nanofabrication techniques such as electron-beam lithography.[14] Figure 1 shows the direct and reciprocal spaces of the 2D periodic and aperiodic structures generated according to Fibonacci, Thue−Morse and Rudin−Shapiro sequences, which exhibit unique spectral features of increasing complexity.[15,16,34–39] These lattices are deterministically generated by a simple constructive algorithm based on the alternation of one-dimensional inflation maps along orthogonal directions.[15,35] This approach uniquely specifies the positions of nanoparticles (black dots) across the arrays once their minimum separation (interparticle distance) has been chosen. As a result, aperiodic nanoparticle arrays are long-range correlated (ordered) structures, despite the lack of translational invariance symmetry. Unlike the simpler case of arrays with multiple periodicity, the calculated diffraction patterns of aperiodic arrays (Figure 1) feature an increasing number of Bragg peaks over imposed to a broad diffuse background. Although for multiple periodic structures the location (in the reciprocal space) of different Bragg peaks can be indexed by simple schemes, this is not possible in quasi-periodic (Fibonacci) and deterministic aperiodic systems. In fact, the diffraction peaks of deterministic aperiodic systems have incommensurate periods[16] and, in the limit of large arrays, densely fill the reciprocal space with characteristic inhomogeneous distributions best described by multifractal analysis.[16,34–39]

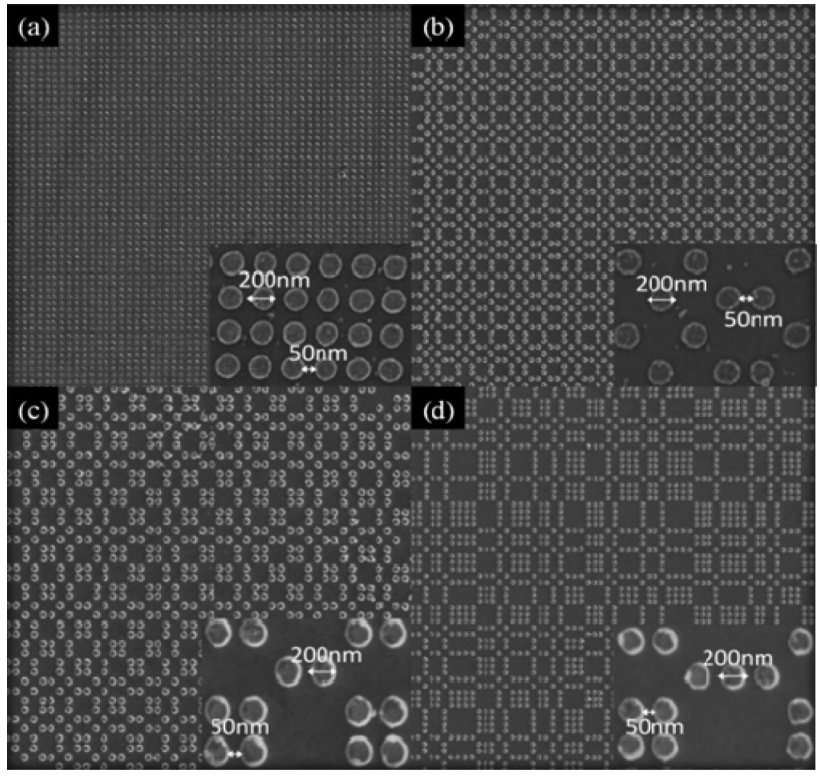

Figure 2. (a) Periodic, (b) Fibonacci, (c) Thue−Morse, and (d) Rudin−Shapiro nanoparticle array. The individual particle sizes are 200 nm, and the minimum interparticle separations in the arrays shown are 50 nm.

The goal of this paper is to systematically investigate the light scattering properties of Fibonacci, Thue−Morse and Rudin−Shapiro nanoparticle arrays fabricated with Electron Beam Lithography (EBL), and to discuss their unique behavior with respect to periodic structures. In particular, by studying a set of samples fabricated with variable (minimum) interparticle separations ranging from 50 to 500 nm we demonstrate that, in contrast to periodic structures, deterministic aperiodic arrays of Au nanoparticles give rise to photonic-plasmonic resonances, which extend across the entire visible spectrum and feature characteristic scattering profiles with highly inhomogeneous intensity distributions. Our experimental results are supported by accurate scattering calculations based on the generalized Mie theory (GMT) approach.

Fabrication of Deterministic Aperiodic Plasmon Lattices. Deterministic aperiodic Au nanoparticle arrays were fabricated using EBL on quartz substrates with a 10 nm layer indium tin oxide (ITO) coating. As detailed elsewhere,[14] our fabrication process flow starts with 180nm of PMMA 950 (Poly Methyl MethAcrylate) spin coated on top of the substrate.

The nanopatterns were written using a Zeiss SUPRA 40VP SEM equipped with Raith beam blanker and NPGS for nanopatterning. After developing the resist in MIBK (methyl isobutyle ketone), a 30 nm thin Au film was deposited on the patterned surface by electron-beam evaporation. The liftoff process was performed using acetone and resulted in the Au nanoparticle arrays shown in Figure 2. The Au particles are cylindrical in shape and their height, as characterized by atomic force microscopy (AFM) and scanning electron microscopy (SEM), was found to be $h = 30$ nm. All the particles have a circular diameter of $d = 200$ nm and a minimum interparticle separation $a = 50$ nm. Following the same fabrication procedure, we fabricated a set of samples with varying minimum interparticle separations ranging between 50 and 500 nm. This effort enabled a systematic study of the influence of the array geometry and dimensionality on the resulting scattering properties. All the arrays were fabricated on the same substrate and have been spaced by approximately 200 μm to avoid undesired cross talks.

Dark-Field Scattering Characterization of Deterministic Aperiodic Arrays. Scattering images of the arrays were recorded using an upright microscope (Olympus BX51 W1). The nanoparticle arrays were immersed in index-matching oil and illuminated with unpolarized white-light from a 100 W tungsten halogen lamp using an oil dark-field condenser (NA = 1.2−1.4) in transmission mode. The light scattered from the arrays was collected with a 40× objective (NA = 0.65) and imaged using a digital camera with an active area of 620 × 580 pixels. The microscope was also equipped with a 150 mm focal length imaging spectrometer (Acton Research, InSpectrum 150) and a back-illuminated CCD detector (Hamamatsu INS-122B) that enabled the spectral analysis of the scattered light using a 150 L/mm grating. The scattering spectra were background corrected by subtraction of the scattering signal from an equal-size, unpatterned adjacent area. The lineshapes of the scattering spectra were additionally corrected by dividing with respect to the normalized spectral line shape of the excitation source.

Experimental Study of Light Scattering from Aperiodic Plasmon Arrays. We perform a systematic study of the dark-field scattering properties of plasmonic arrays with different geometries and interparticle separations. In general, it has

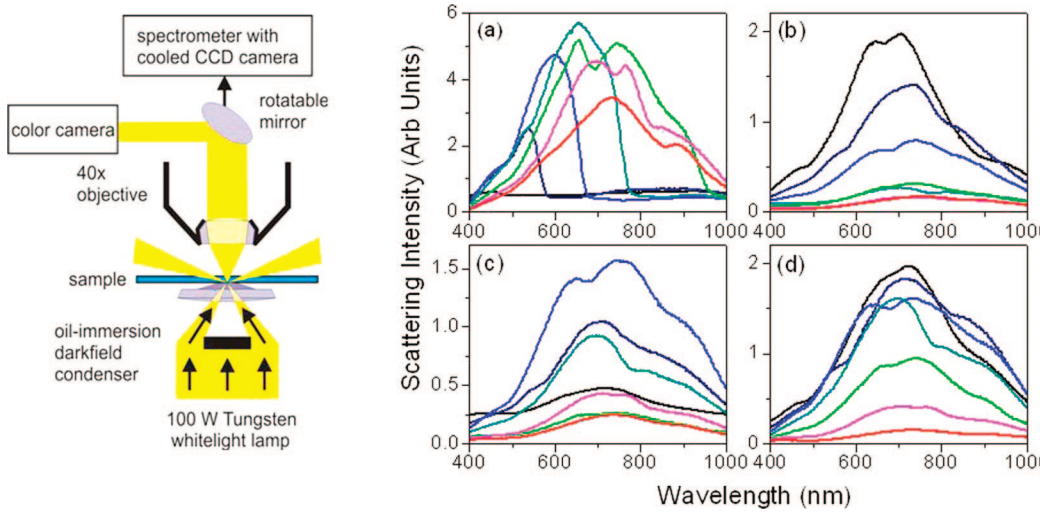

Figure 3. Measured scattering as a function of the wavelength for 2-D arrays of Au nanoparticles with radii of 100 nm: (a) periodic, (b) Fibonacci, (c) Thue−Morse, and (d) Rudin−Shapiro, and varied minimum separation distances: 50 nm (black), 100 nm (navy), 150 nm (blue), 200 nm (dark cyan), 300 nm (green), 400 nm (magenta) and 500 nm (red). The varying intensity plateaus at around 400 nm arise from different filling fractions of the arrays. Taking into account the collection angle of the objective (40.5°) and the cone of total internal reflection (39.0°), we estimate that we collect 17% of the scattered light. The dark field scattering setup used in the measurements is also shown.

been shown [40–44] that two separate electromagnetic regimes govern the optical response of periodic metal-nanoparticle arrays: near- and far-field coupling. When dipolar particles are separated by very short distances, up to approximately $D \approx 1/k_0 = \lambda_0/2\pi$ (k_0 and λ_0 being the free-space wavenumber and the wavelength, respectively), quasi-static near-field interactions dominate the collective response of the arrays, and localized plasmon modes with strongly enhanced local fields can be excited. On the other extreme, when particles are spaced by larger distances, long-range far-field electromagnetic interactions, mediated by diffracted optical waves, strongly affect the plasmonic response of the arrays.

An accurate diffraction theory of periodic metal gratings (arrays) has been recently developed by Meier at al.[44–46] According to this theory, dipolar coupling leads to the in-phase superposition of the incident and the fields radiated by the individual nanoparticles in the plane of the array. In particular, periodic arrays of spatial period (grating constant) Δ radiate at different grating orders m for a critical grating constant Δ_C which satisfies the equation:[44]

$$\Delta_C = m\lambda_0/(n_1 \sin \varphi + n_2) \quad (1)$$

where ϕ is the light incident angle in the medium of refractive index n_1, n_2 is the refractive index of the array substrate, and m is an integer defining the grating order. When the grating constant remains below the critical value ($\Delta < \Delta_C$), the optical resonance of the grating (for the first grating order, $m = 1$) corresponds to that of the individual particles with reduced radiation damping. For values of the grating constants approaching the critical value Δ_C, the plasmonic modes start to radiate in the array plane, leading to a stronger coupling between particles, which causes the red shift of the plasmon resonance. According to this picture, when a particle array of lattice constant Δ is illuminated by a white light source, some grating orders will radiate at grazing angle in accordance with eq 1. However, when the incident wavelength coincides with the localized surface plasmon wavelength, the radiated light fields strongly couple to the individual nanoparticle plasmon fields and lead to the excitation of hybrid photonic-plasmonic resonances. These resonances have first been observed in 1D arrays of gold nanoparticles using dark-field spectroscopy.[40] The existence of very sharp photonic-plasmonic resonances in periodic arrays of metal nanoparticles was recently predicted by Haynes et al., and experimentally confirmed in periodic two-dimensional gold nanoparticles arrays.[44]

It is therefore interesting to compare the formation of photonic-plasmonic resonances in periodic and deterministic aperiodic structures. The scattering spectra measured for periodic square lattices with interparticle separations ranging from 50 to 500 nm are shown in Figure 3a. Because we are only interested in discussing plasmonic spectral shifts originating from the different arrays geometries, we have not corrected the scattered intensities shown in Figure 3 by the different filling fractions of the arrays, which specifically depend on the array geometry and the minimum interparticle separations. We also point out that we were able to observe grating-induced plasmon modes only when the arrays were immersed in an index matching oil. In fact, as previously reported,[40–44] a close matching of the refractive indices of the substrate material (ITO) and the superstratum is required to ensure proper phase-matching of plasmon modes propagating parallel to the top and bottom interfaces. Under these conditions, the plasmon peak moves to longer wavelengths (red shift) and broadens with increasing interparticle separation. According to Meier's theory,[44–46] the red shift of the plasmon peak observed in periodic arrays of metal nanoparticles when increasing their separations can be attributed to the effect of dipolar coupling. In addition, satellite scattering peaks, which are attributed to the excitation of photonic-plasmonic resonances, appear at specific lattice configurations and gradually move to longer wavelengths within the scattering spectra as the interparticle separations

are increased from 300 to 500 nm. The appearance of these satellite peaks in periodic structures is in agreement with eq 1, which predicts the excitation of the first order ($m = 1$) photonic-plasmon resonances for grating constants $\Delta > \Delta_C \approx 200$ nm. When the grating constants of the arrays are increased beyond Δ_C, these resonances red shift within the scattering spectra and their intensities become weaker, as a consequence of the increased detuning with respect to the individual nanoparticles plasmon peaks.

On the other hand, the scattering spectra of the aperiodic structures, measured under identical conditions, are shown in Figure 3b−d for Fibonacci, Thue−Morse and Rudin−Shapiro arrays, respectively. The minimum interparticle separation in these lattices matches the grating constant of the reference periodic structures. However, differently from the case of periodic structures, the results shown in Figure 3b−d demonstrate that the scattering spectra become progressively broader, and extend across the entire visible range, as the arrays complexity increases for Fibonacci, Thue−Morse and Rudin−Shapiro structures. Interestingly, we conclude that the contributions of grating-induced scattering resonances can also be observed in deterministic aperiodic structures (Figures 3b−d), despite their lack of global periodicity (see Figure 1). However, the lack of translational invariance, which characterizes aperiodic plasmonic structures, makes the definition of a simple diffraction relation, such as the one expressed by eq 1, impossible. In fact, one can approximately regard aperiodic arrays as derived from an inhomogeneous distribution of effective grating constants corresponding to the most represented spatial periods in the structures, manifested by the dominant diffraction peaks shown in Figure 1. This leads to the possibility of fulfilling simultaneous resonance conditions for the excitation of photonic-plasmonic resonances in deterministic aperiodic structures. According to this qualitative picture, the inhomogeneously broadened scattering spectra observed in Figure 3 reflect the superposition of a large number of grating-induced photonic-plasmonic resonances of different orders and it becomes clear that the observed scattering spectra progressively broaden along the array series: periodic, Fibonacci, Thue−Morse and Rudin−Shapiro. This intuitive picture will be justified in the computational section of this paper based on accurate GMT calculations of scattering from periodic and aperiodic nanoparticle arrays.

Far-Field Scattering Maps. In the previous section we have discussed the resonant nature of the in-plane multiple photonic-plasmonic resonances which can be excited in diffractively coupled (dipolar coupling) metal nanoparticle arrays. The plasmonic scattering response of nanoparticle arrays coupled by long-range dipolar interactions are vividly illustrated by looking at the far-field images of resonantly excited plasmonic arrays. The scattering images of aperiodic arrays illuminated using white light exhibit characteristic inhomogeneous spatial distributions of the different light components (see Figure 4). The spatial light distribution captured in these scattering images critically depends on the geometry and the minimum interparticle separations in the patterns.

It interesting to notice that the scattering maps shown in Figure 4 were obtained using incoherent radiation (tungsten halogen lamp), whose coherence length can be estimated in the order of 5 μm, which is much smaller than the lateral dimension of the arrays. Therefore, in-plane multiple light scattering of fewer neighboring Au nanoparticles compared to the total number of array particles is enough to give rise to the scattering response experimentally observed in Figure 4.

Figure 4 demonstrates that, different from aperiodic structures, the high degree of structural correlation typical of periodic arrays induces scattering states at well-defined wavelengths (colors), which correspond to radiative photonic-plasmonic resonances associated to the periodicity of the arrays. In particular, as expected in the regime of dipolar coupling, larger grating constants (particle separations) correspond to the resonances of longer wavelengths (Figure 4a1−a4). As a result, the scattered color of periodic Au nanoparticle arrays can be conveniently controlled by the interparticle separations, in agreement with the spectral results shown in Figure 3. In contrast, the scattering maps of deterministic aperiodic arrays exhibit highly inhomogeneous scattered intensity patterns, which depend sensitively on the interparticle separations. For small interparticle separations (<300 nm), multiple light scattering in aperiodic structures (dipolar coupling) leads to the formation of a highly structured spatial distribution of visible colors. We notice that the color distributions observed at small particle separations in aperiodic lattices do not directly reflect the Fourier spectrum of the arrays structures, as expected by simple Fourier optics. In fact, the resonant character of the arrays and the importance of particle coupling[15] can only be explained by an accurate electrodynamics approach.

Computational Analysis of Light Scattering from Aperiodic Plasmon Arrays. The understanding of the complex electromagnetic and plasmon coupling in large nanoparticle arrays without translational invariance provides significant challenges to the numerical simulation methods of classical electrodynamics theory. A majority of recent numerical studies of the scattering from isolated nanoparticles, nanoparticle arrays and aggregates rely on simple yet flexible approximate techniques such as the discrete dipole approximation (DDA)[47] and the coupled-dipole approach (CDA).[48] However, the use of more accurate methods, i.e., the multiple multipole method (MMP)[49] or the generalized multiparticle Mie theory (GMT) [50–53] is necessary to include multipolar scattering terms in the analysis and to account for all the mutual interactions within the array. This is especially important if the arrays are composed of larger nanoparticles and higher-order multipole interactions contribute noticeably to the array electromagnetic response.

In the following, we use the rigorous GMT approach[50–54] to provide a support and interpretation of our experimental data. Being formulated in the complex domain, GMT can be conveniently applied to study plasmonic structures with realistic material losses. Although the application domain of GMT is restricted to spherical scatterers, it yields the analytical solution of the scattering problem and results in

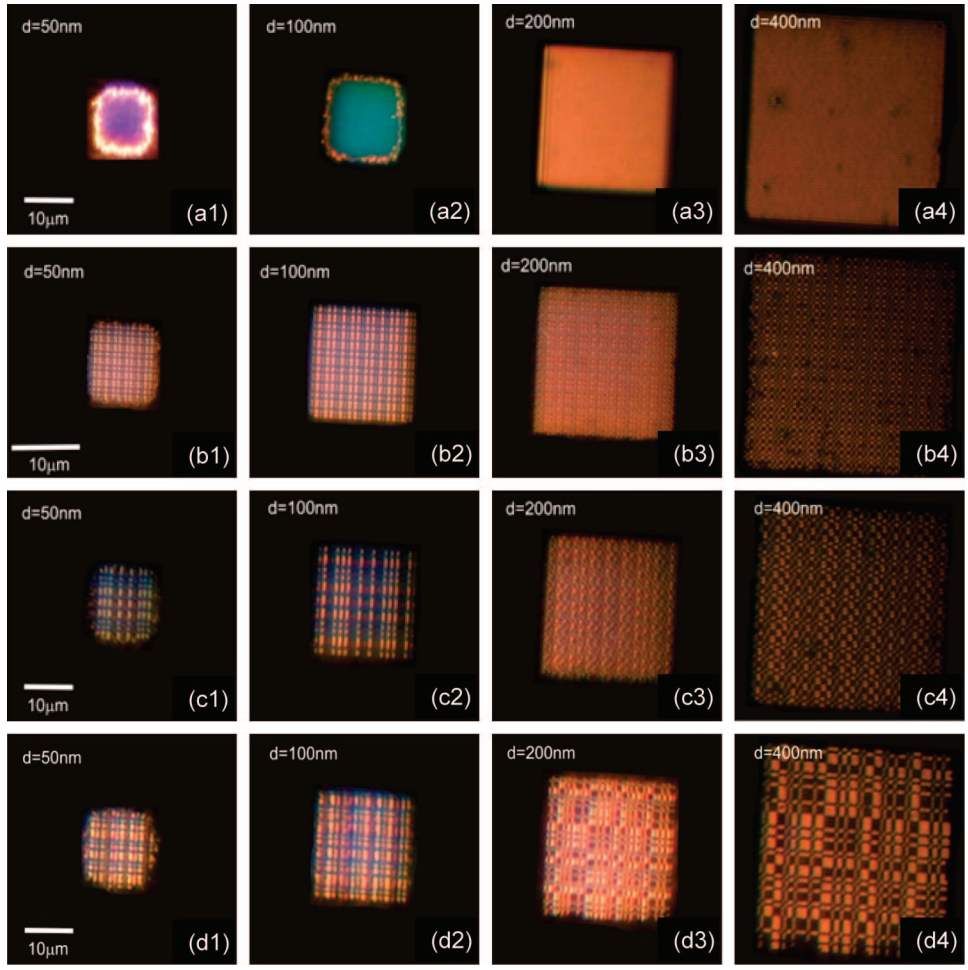

Figure 4. Scattering maps of periodic (a1−a4), Fibonacci (b1−b4), Thue−Morse (c1−c4) and Rudin−Shapiro (d1−d4) nanoparticle arrays with different interparticle separations, as indicated in the figure. The scattering pictures are in true colors. We notice that red-shifted scattering occurs from the edge regions of the arrays, as a consequence of fabrication imperfections due to partial liftoff. These liftoff problems are particularly pronounced in the arrays with the smallest interparticle separation, as evident in panels a1, b1, c1, and d1.

highly efficient algorithms. Because the main focus of this study is to reveal the role of the array morphology on its scattering characteristics, GMT can be used as a very efficient simulation tool, and we demonstrate that it captures the major features of the scattering from periodic and aperiodic arrays. Shapes of individual nanoparticles may be introduced in the analysis (e.g., by using a more general MMP approach[49]) as additional design parameters; however, this is a subject of a separate study.

In the frame of GMT approach, the electromagnetic field in a photonic structure of L nanoparticles can be constructed as a superposition of partial fields scattered from each particle. These partial scattered fields as well as the incident field and internal fields are expanded in the orthogonal basis of vector spherical harmonics represented in local coordinate systems associated with individual particles:

$$E_{sc}^{l} = \sum_{n=1}^{\infty} \sum_{m=-n}^{n} (a_{mn}^{l} N_{mn} + b_{mn}^{l} M_{mn}) \qquad l = 1, ..., L \qquad (2)$$

The use of the powerful addition (translation) theorem for vector spherical harmonics enables the transformation (translation) of the series expansion for the partial fields of the lth particle into an expansion in the local coordinate system associated with any other particle of the array. A general matrix equation for the Lorenz−Mie multipole scattering coefficients (a_{mn}^{l}, b_{mn}^{l}) can be obtained by imposing the electromagnetic boundary conditions for the tangential components of the electric and magnetic fields and by truncating the infinite series expansions to a maximum multipolar order N:

$$a_{mn}^{l} + \tilde{a}_{n}^{l} \sum_{j \neq l}^{(1,L)} \sum_{\nu=1}^{N} \sum_{\mu=-\nu}^{\nu} (A_{mn\mu\nu}^{jl} a_{\mu\nu}^{j} + B_{mn\mu\nu}^{jl} b_{\mu\nu}^{j}) = \tilde{a}_{n}^{l} p_{mn}^{l} \qquad (3a)$$

$$b_{mn}^{l} + \tilde{b}_{n}^{l} \sum_{j \neq l}^{(1,L)} \sum_{\nu=1}^{N} \sum_{\mu=-\nu}^{\nu} (B_{mn\mu\nu}^{jl} a_{\mu\nu}^{j} + A_{mn\mu\nu}^{jl} b_{\mu\nu}^{j}) = \tilde{b}_{n}^{l} q_{mn}^{l} \qquad (3b)$$

Here, $A_{mn\mu\nu}{}^{jl}$, $B_{mn\mu\nu}{}^{jl}$ are the translation matrices, which only depend on the distance and direction of translation from origin l to origin j;[50−53] $\tilde{a}_{n}^{l}$, $\tilde{b}_{n}^{l}$ are the Mie scattering coefficients of lth sphere in the free space;[54] and p_{mn}^{l}, q_{mn}^{l} are the expansion coefficients of the incident field. Once truncated matrix eqs 3 are solved for the scattering coefficients, the scattering, extinction and absorption cross-sections as well as the scattered field distributions can be accurately calculated at any desired level of accuracy. The number of the multipolar terms kept in the sphere-centered expansions of the electromagnetic fields in eqs 3a and 3b

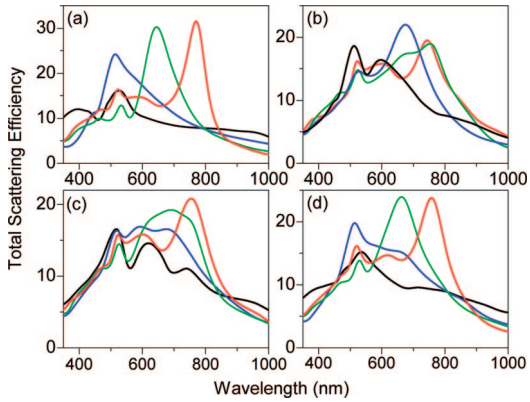

Figure 5. Total calculated scattering efficiency as a function of the wavelength for 2-D finite-size arrays of Au spherical nanoparticles with radii of 100 nm: (a) periodic ($L = 100$), (b) Fibonacci ($L = 80$), (c) Thue−Morse ($L = 128$), and (d) Rudin−Shapiro ($L = 120$). Minimum separation distances: 50 nm (black), 150 nm (blue), 300 nm (green), and 500 nm (red).

were estimated by using the Wiscombe criterion $N \approx ka + 4(ka)^{1/3} + 2$ (a is the sphere radius),[54] and the relative residual error tolerance in the numerical solution was set at the level of 10^{-7}.

Figure 5 shows the GMT-calculated total scattering efficiencies (Q_{sc}) for an unpolarized light field normally incident on the finite-size arrays composed of $L \sim 100$ nanospheres. The scattering efficiency is defined with respect to the volume mean radius of the array $a_c = (3V_c/4\pi)^{1/3}$ such as $Q_{sc} = C_{sc}/\pi a^2$, where C_{sc} is the scattering cross-section[54] and V_c is the combined volume of all the spheres in the array. The Au nanoparticle dispersion is modeled by using the Drude formula for gold with parameters introduced in ref 55. As can be seen in Figure 5, our GMT calculations are able to reproduce the broad scattering response experimentally observed in the investigated arrays of metal nanoparticles. In agreement with experimental data shown in Figure 3, frequency scans of scattering efficiency of periodic arrays feature a major peak associated with the dipole plasmon resonance, which is progressively red-shifted with the increase of the array period. For larger separations, higher-order photonic-plasmonic resonances appear in the array spectrum. In contrast, scattering spectra of aperiodic structures show multiple peaks across the visible spectral range, which are associated with the excitation of multiple photonic-plasmonic scattering resonances due to electromagnetic coupling at multiple length scales. As explained above, the experimental plots in Figure 3 have not been normalized to the actual value of forward scattering intensity associated with various array filling fractions, which explains markedly different levels of efficiency observed in experimental and theoretical curves.

On the other hand, more pronounced (with respect to experimental data in Figure 3) resonant features observed in Figure 5 can be explained by the fact that the material dispersion model[55] underestimates losses in gold. However, observation of multiple well-defined resonance peaks in the simulated scattered spectra provides an insight into the formation of a broad scattering response of aperiodic arrays. Indeed, higher material losses in fabricated structures result

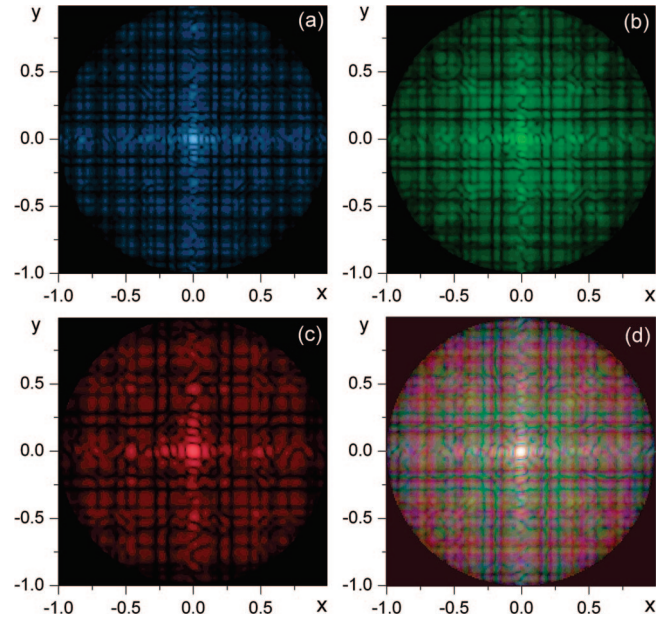

Figure 6. Scattering maps (angular distributions of the scattering intensity) for the forward scattering hemisphere ($0 \le \theta \le \pi$, $0 \le \phi \le 2\pi$) for a Rudin−Shapiro array ($L = 512$) at three different wavelengths corresponding to the resonant peaks observed in Figure 5d: $\lambda = 457$ nm (a), $\lambda = 515$ nm (b), $\lambda = 662$ nm (c), and their incoherent mixture (d). Minimum separation distances are 100 nm. The scattering angles can be calculated from the x- and y-axes values as $\cos^2\theta = \max\{0,1-x^2-y^2\}$, $\phi = \tan^{-1}(y/x)$.

in broadening of their scattering spectra, disappearance of individual peaks and formation of a broadband frequency response as observed in the experimental data in Figure 3. We emphasize that the observed broadband response is a result of a collective effect of excitation of multiple photonic-plasmonic resonances due to the presence of multiple length scales in the arrays of identical particles rather than the excitation of plasmonic resonances in random structures composed of particles of different shapes and sizes, each having its own resonant frequency, as previously observed.[56]

Finally, with the goal of providing a quantitative justification to the data shown in Figure 4, we studied the angular distribution of the intensity of the electromagnetic field scattered from aperiodic nanoparticles arrays. We chose the Rudin−Shapiro array as a test example, because it possesses the highest structural complexity and can potentially reveal most unusual features of the scattered field angular distribution. Figure 6 presents the projection of the Z_{11} element of the scattering matrix[54] onto the forward scattering hemisphere for the case of the normal incidence of an unpolarized plane wave on the Rudin−Shapiro array composed of 512 nanoparticles with a minimum separation of 100 nm. The value of Z_{11} element is found as a sum of magnitudes of the elements of the amplitude scattering matrix, $Z_{11} = {}^1/_2(|S_1|^2 + |S_2|^2 + |S_3|^2 + |S_4|^2)$, and for an unpolarized incident field it determines the angular distribution of the scattered intensity.[54] The convention of Bohren and Huffman[54] was used to specify the amplitude scattering matrix elements, and the center of the forward-scattering hemisphere corresponds to the propagation direction of the incident field. Panels a−c of Figure 6 show the angular intensity distributions for the

scattering at three different wavelengths corresponding to the most pronounced resonant peaks observed in the frequency spectrum plotted in Figure 5d. These wavelengths fall within the blue, green, and red parts of the visible spectrum, respectively. It can be seen in Figure 6 that all three scattering maps demonstrate a very complex and structured angular distribution of the scattered intensity. We also observe that most of the light incident on the structure is forward scattered, which is manifested by the bright spots in the centers of the scattering maps. It should be noted, however, that this forward-scattered intensity was not collected in our experimental measurements done with the dark-field scattering setup due to the oblique illumination angle. In the attempt to predict the scattering response of the structure under the broadband incoherent light illumination, we computed the incoherent sum (intensity addition) of the three scattering maps and plotted the result in Figure 6d. The resulting picture reveals a highly structured angular distribution of colors in the scattering response of the Rudin−Shapiro array, in good qualitative agreement with the experimentally measured scattering map distribution shown in Figure 4d2.

We believe that the control of highly structured scattering resonances in deterministic aperiodic arrays of metal nanoparticles can open alternative routes for the fabrication of novel plasmonic devices based on scattered color change.

Conclusions. By combining experimental dark-field scattering spectroscopy and accurate electrodynamics calculations, we have investigated the scattering properties of two-dimensional plasmonic lattices based on the concept of deterministic aperiodicity. In particular, we have discussed visible light scattering from Fibonacci, Thue−Morse and Rudin−Shapiro lattices fabricated by electron-beam lithography on transparent quartz substrates. We have demonstrated that deterministic aperiodic Au nanoparticle arrays give rise to broad plasmonic resonances spanning the entire visible spectrum, in good agreement with accurate electrodynamics calculations based on the generalized Mie theory. Finally, we have shown that far-field diffractive coupling in deterministic aperiodic structures leads to the formation of characteristic photonic-plasmonic modes with spatially inhomogeneous scattering profiles. The engineering of deterministic aperiodic metal nanoparticle arrays with distinctive plasmonic scattering resonances can lead to the fabrication of novel broadband optical devices such as plasmonic-enhanced biosensors, improved substrates for surface-enhancement Raman scattering (SERS) and plasmonic arrays for enhanced light extraction in light emitting diodes (LEDs).

Acknowledgment. This work was partially supported by the College of Engineering Dean's Catalyst Award and the U.S. Army Research Laboratory through the project: *Development of novel SERS substrates via "rationally" designed nanofabrication strategies.* We thank Dr. Y.-L. Xu and Dr. D. W. Mackowski for making their GMT Fortran codes publicly available.

References

(1) Luck, J. M. Cantor spectra and scaling of gap widths in deterministic aperiodic systems. *Phys. Rev. B* **1989**, *39*, 5834.
(2) Queffélec, M. *Substitution dynamical systems-spectral analysis*; Lecture Notes in Mathematics, vol. 1294; Springer: Berlin, 1987.
(3) Dulea, M.; Johansson, M.; Riklund, R. Localization of electrons and electromagnetic waves in a deterministic aperiodic system. *Phys. Rev. B* **1992**, *45*, 1051.
(4) Macia, E. The role of aperiodic order in science and technology. *Rep. Prog. Phys.* **2006**, *69*, 397.
(5) Rudinger, A.; Piechon, F. On the multifractal spectrum of the Fibonacci chain. *J. Phys. A.: Math. Gen.* **1998**, *31*, 155–164.
(6) *Symbolic dynamics and its applications*; Williams, Susan G. , Ed.; American Mathematical Society, Providence, RI, 2004; ISBN 0821831577.
(7) *Number theory in science and communication*; Schroeder, M. R., Ed.; Springer-Verlag: Berlin, 1985.
(8) *The algorithmic beauty of plants*; Prusinkiewicz, P., Lindenmayer, A., Eds.; Springer Verlag: New York, 1990.
(9) Capaz, R. B.; Koiller, B.; de Queiroz, S. L. A. Gap states and localization properties of one-dimensional Fibonacci quasicrystals. *Phys. Rev. B* **1990**, *42*, 6402.
(10) Kohmoto, M.; Sutherland, B.; Tang, C. Critical wave functions and a Cantor-set spectrum of a one-dimensional quasicrystal model. *Phys. Rev. B* **1987**, *35*, 1020–1033.
(11) Maciá, E. Physical nature of critical modes in Fibonacci quasicrystals. *Phys. Rev. B* **1999**, *60*, 10032.
(12) Craciun, F.; Bettucci, A.; Molinari, E.; Petri, A.; Alippi., A. Direct experimental observation of fracton mode patterns in one dimensional Cantor composite. *Phys. Rev. Lett.* **1992**, *68*, 342–347.
(13) Dal Negro, L.; Feng, N. N. Spectral gaps and mode localization in Fibonacci chains of metal nanoparticles. *Opt. Exp.* **2007**, *15*, 22–14396.
(14) Dallapiccola, R.; Gopinath, A.; Stellacci, F.; Dal Negro, L. Quasi-periodic distribution of plasmon modes in two-dimensional Fibonacci arrays of metal nanoparticles. *Opt. Exp.* **2008**, *16*, 8–5544.
(15) Dal Negro, L.; Feng, N. N.; Gopinath, A. Electromagnetic coupling and plasmon localization in deterministic aperiodic arrays. *J. Opt. A: Pure Appl. Opt.* **2008**, *10*, 064013.
(16) *Quasicrystals: a primer*, 2nd edition; Janot, C., Ed. Oxford University Press: Oxford, U.K., 1997.
(17) Gellermann, W.; Kohmoto, M.; Southerland, B.; Taylor, P. C. Localization of light waves in Fibonacci dielectric multilayers. *Phys. Rev. Lett.* **1993**, *72*, 633.
(18) Kohmoto, M.; Sutherland, B.; Iguchi, K. Localization in optics: quasiperiodic media. *Phys. Rev. Lett.* **1987**, *58*, 2436–2438.
(19) Huang, X. Q.; Jiang, S. S.; Peng, R. W.; Hu, A. Perfect transmission and self-similar optical transmission spectra in symmetric Fibonacci-class multilayers. *Phys. Rev. B* **2001**, *63*, 245104.
(20) Dutta Gupta, S.; Ray, D. S. Optical multistability in a nonlinear Fibonacci multilayer. *Phys. Rev. B* **1988**, *38*, 5–3628.
(21) Dal Negro, L.; Oton, C. J.; Gaburro, Z.; Pavesi, L.; Johnson, P.; Lagendijk, Ad.; Righini, R.; Colocci, M.; Wiersma, D. Light transport through the band-edge states of Fibonacci quasicrystals. *Phys. Rev. Lett.* **2003**, *vol 90*, 0555015.
(22) Ghulinyan, M.; Oton, C. J.; Dal Negro, L.; Pavesi, L.; Sapienza, R.; Colocci, M.; Wiersma, D. Light pulse propagation in Fibonacci quasicrystals. *Phys. Rev. B* **2005**, *71*, 094204.
(23) Morse, M. Recurrent geodesics on a surface of negative curvature. *Trans. Am. Math. Soc.* **1921**, *22*, 84.
(24) Pikovsky, A. S.; Zaks, M. A.; Feudel, U.; Kurths, J. Singular continuous spectra in dissipative dynamics. *Phys. Rev. E* **1995**, *52*, 285.
(25) Cheng, S.-F.; Jin, G.-J. Trace map and eigenstates of a TM chain in a general model. *Phys. Rev. B* **2002**, *65*, 134206.
(26) Koláø, M.; Ali, M. K.; Nori, F. Generalized Thue−Morse chains and their physical properties. *Phys. Rev. B* **1991**, *43*, 1034.
(27) Liu, N. Propagation of light waves in Thue−Morse dielectric multilayers. *Phys. Rev. B* **1997**, *55*, 3543.
(28) Dal Negro, L.; Stolfi, M.; Yi, Y.; Michel, J.; Duan, X.; Kimerling, L. C.; LeBlanc, J.; Haavisto, J. Photon bandgap properties and omnidirectional reflectance in Si/SiO_2 Thue−Morse quasicrystals. *Appl. Phys. Lett.* **2004**, *84*, 25–5186.
(29) Dal Negro, L.; Yi, J. H.; Yi, Y.; Nguyen, V.; Michel, J.; Kimerling, L. C. Spectrally enhanced light emission from aperiodic photonic structures. *Appl. Phys. Lett.* **2005**, *86*, 261905.
(30) Igì; oi, F.; Turban, L.; Rieger, H. Anomalous diffusion in aperiodic environments. *Phys. Rev. E* **1999**, *59*, 2–1465.
(31) Pièchon, F. Anomalous diffusion properties of wave packets on quasiperiodic chains. *Phys. Rev. Lett.* **1996**, *76*, 23–4372.
(32) Kroon, L.; Lennholm, E.; Riklund, R. Localization-delocalization in aperiodic systems. *Phys. Rev. B* **2002**, *66*, 094204.

(33) Kroon, L.; Riklund, R. Absence of localization in a model with correlation me asure as a random lattice. *Phys. Rev. B* **2004**, *69*, 094204.
(34) Fu, X.; Liu, Y.; Cheng, B.; Zheng, D. Spectral structure of two-dimensional Fibonacci quasilattices. *Phys. Rev. B* **1991**, *43*, 10808.
(35) Ferralis, N.; Szmodis, A. W.; Diehl, R. D. Diffraction from one and two dimensional quasicrystalline gratings. *Am. J. Phys.* **2004**, *72*, 1241.
(36) Cheng, Z.; Savit, R.; Merlin, R. Structure and electronic properties of Thue−Morse lattices. *Phys. Rev. B* **1988**, *37*, 4375.
(37) Axel, F.; Terauchi, H. High-resolution X-ray diffraction spectra of Thue−Morse GaAs-AlAs heterostructures: towards a novel description of disorder. *Phys. Rev. Lett.* **1991**, *66*, 2223.
(38) Godreche, C.; Luck, J. M. Multifractal analysis in reciprocal space and the nature of the Fourier transform of self-similar structures. *J. Phys. A: Math., Gen.* **1990**, *23*, 3769.
(39) Liviotti, E. A study of the structure factor of Thue−Morse and period-doubling chains by wavelet analysis. *J. Phys.: Condens. Matter* **1996**, *8*, 5007.
(40) Hicks, E. M.; Zou, S.; Schatz, G. C.; Spears, K. G.; VanDuyne, R. P.; Gunnarson, L.; Rindzevicius, T.; Kasemo, B.; Kall, M. Controlling plasmon line shapes through diffractive coupling in linear arrays of cylindrical nanoparticles fabricated by electron beam lithography. *Nano Lett.* **2005**, *5*, 1065.
(41) Zhao, L. L.; Kelly, K. L.; Schatz, G. C. The extinction spectra of silver nanoparticle arrays: influence of array structure on plasmon resonant wavelength and width. *J. Phys. Chem. B* **2003**, *107*, 7343.
(42) Bouhelier, A.; Bachelot, R.; Im, J. S.; Wiederrecht, G. P.; Lerondel, G.; Kostcheev, S.; Royer, P. *Electromagnetic interactions in plasmonic nanoparticle arrays*. *J. Phys. Chem. B* **2005**, *109*, 3195.
(43) Lamprecht, B.; Schider, G.; Lechner, R. T.; Ditlbacher, H.; Krenn, J. R.; Leitner, A.; Aussenegg, F. R. Metal nanoparticle gratings: influence of dipolar particle interaction on the plasmon resonance. *Phys. Rev. Lett.* **2000**, *84*, 20–4721.
(44) Felidj, N.; Laurent, G.; Aubard, J.; Levi, G.; Hohenau, A.; Krenn, J. R.; Aussenegg, F. R. Grating-induced plasmon modes in gold nanoparticle arrays. *J. Chem. Phys.* **2005**, *123*, 221103.
(45) Meier, M.; Wokaun, A.; Liao, P. F. Enhanced fields on rough surfaces: dipolar interactions among particles of sizes exceeding the Rayleigh limit. *J. Opt. Soc. Am. B* **1985**, *2*, 931.
(46) Carron, K. T.; Fluhr, W.; Meier, M.; Wokaun, A.; Lehmann, H. W. Resonances of two-dimensional particle gratings in surface-enhanced Raman scattering. *J. Opt. Soc. Am. B.* **1986**, *3*, 430.
(47) Draine, B. T. The discrete-dipole approximation and its applications to interstellar graphite grains. *Astrophys. J.* **1988**, *333*, 848.
(48) Purcell, E. M.; Pennypacker, C. R. Scattering and absorption of light by nonspherical dielectric grains. *Astrophys. J.* **1973**, *186*, 705.
(49) Ballisti, R.; Hafner, C. The multiple multipole method in electro- and magnetostatic problems. *IEEE Trans. Magn.* **1983**, *19*, 2367.
(50) Quinten, M.; Kreibig, U. Absorption and elastic-scattering of light by particle aggregates. *Appl. Opt.* **1993**, *32*, 6173.
(51) Mackowski, D. W. Calculation of total cross-sections of multiple sphere clusters. *J. Opt. Soc. Am. A* **1994**, *11*, 2851.
(52) Xu, Y.-L. Electromagnetic scattering by an aggregate of spheres. *Appl. Opt.* **1995**, *34*, 4573.
(53) *Optical properties of metal clusters*; Kreibigv, U., Vollme, M., Eds.; Springer-Verlag, Berlin, 1995.
(54) *Absorption and scattering of light by small particles*; Bohren, C. F., Huffman, D. R., Eds.;Wiley-VCH, New York, 1998.
(55) Maier, S. A.; Kik, P. G.; Atwater, H. A. Optical pulse propagation in metal nanoparticle chain waveguides. *Phys. Rev. B* **2003**, *67*, 20540.
(56) Podolskiy, V. A.; Sarychev, A. K.; Narimanov, E. E.; Shalaev, V. M. Resonant light interaction with plasmonic nanowire systems. *J. Opt. A: Pure Appl. Opt.* **2005**, *7*, S323.

NL8013692